

Simplifying and Interpreting Two-Tone Measurements

Kate A. Remley, *Member, IEEE*, Dylan F. Williams, *Fellow, IEEE*,
Dominique M. M.-P. Schreurs, *Senior Member, IEEE*, and John Wood, *Senior Member, IEEE*

Abstract—We develop a mathematical description of the response of weakly nonlinear systems to second-order memory mechanisms. Our description is based on a time-varying gain-modulation function. We show that intermodulation (IM) products arising from interactions at baseband have phase symmetries different from both interactions at second harmonic frequencies and gain compression and, thus, may be readily distinguished through measurement. We also demonstrate a technique for measuring and aligning the phase of IM products outside the measurement bandwidth of our instrumentation to identify contributions to memory with broad frequency response.

Index Terms—Gain modulation, intermodulation (IM) distortion, large-signal network analyzer, memory effects, nonlinear vector network analyzer (NVNA), two-tone measurements.

I. INTRODUCTION

WE DEVELOP a general and intuitive mathematical description of the third-order intermodulation (IM3) behavior of amplifier circuits under two-tone excitation. We represent the response of the nonlinear amplifier circuit in terms of a time-varying second-order function that modulates the gain of the amplifier. This gain modulation produces IM3 distortion on both RF and IF time scales. Our description aids in understanding the sources of this distortion, also called “memory,” as illustrated through measurements of several representative amplifier circuits.

The concept of a distinct time-varying function that describes the behavior of an amplifier with memory has been discussed in several publications, including [1]–[5]. Several of these papers derive filter functions that act on the baseband envelope to represent memory effects for use in two- or three-box Wiener–Hammerstein-type models. Alternatively, [4] and [5] represent baseband long-term memory effects in terms of a time-varying gain modulating function. In [4], a circuit-specific gain function is extracted from direct measurement, while in [5], various excitation signals are used to extract the gain function indirectly. In these papers, the gain function is then used in behavioral modeling and/or amplifier predistortion.

Here, we generalize the form of the gain function to include all second-order effects, including those acting at baseband and at the second harmonic. Our goal is different as well: we use our

description to mathematically identify and distinguish between the origins of IM3 distortion created by RF and IF time-scale memory-inducing mechanisms under two-tone excitation.

Our straightforward device-independent mathematical description offers a unified explanation for the IM3 phase distortion behavior reported in [6]–[10]. These references draw several conclusions: while IM3 arising strictly from time-independent gain compression results in IM3 products whose magnitudes and phases have even symmetry (upper and lower IM3 products having the same magnitudes and phases), baseband mechanisms result in IM3 products with odd symmetry (equal magnitudes and opposite-sign phases having the same absolute value). In addition, IM3 products arising from second harmonic mechanisms have magnitudes and phases with even symmetry when the terminating impedances are equal. This is usually achieved for the narrow-band case. Finally, when there is no dominant IM3 mechanism, these symmetries can be destroyed.

We validate our mathematical description by demonstrating these symmetries through large-signal measurements of various amplifier circuits. We use a nonlinear vector network analyzer (NVNA) [11] to obtain calibrated measurements of both magnitude and relative phase of the IM3 products, and use a post-processing routine [12] for in-band relative phase alignment.

The NVNA can simplify two-tone relative-phase measurements compared to methods presented in [7]–[9], [13], and [14]. However, its use is often restricted to measurements where all frequency components fall within a limited IF measurement bandwidth, 8 MHz for currently available instruments. To enable identification of sources of memory with frequency response broader than our IF bandwidth, we utilize a new technique that extends the measurement bandwidth of our NVNA.

II. IM DISTORTION AND MEMORY EFFECTS

When an amplifier is excited by multiple frequencies and driven into its nonlinear operating range, it generates numerous mixing products. These additional frequency components are generated both at baseband and at the harmonics of the excitation, as well as at the excitation frequencies themselves. Mixing may subsequently occur between the harmonically generated frequency components and the original excitation signals, creating “intermodulation (IM) distortion” products [15], [16]. For example, an amplifier driven by signals at frequencies ω_1 and ω_2 will generate IM3 products at the frequencies $2\omega_1 - \omega_2$ and $2\omega_2 - \omega_1$. (The “third-order” designation arises from a common representation of the transfer function of an amplifier as a simple power series. The third-degree term in this power series, often arising from simple gain compression, includes frequency components at $2\omega_1 - \omega_2$ and $2\omega_2 - \omega_1$.)

Manuscript received April 24, 2004; revised July 15, 2004. Work partially supported by the U.S. Government not subject to U.S. copyright.

K. A. Remley and D. F. Williams are with the National Institute of Standards and Technology, Boulder, CO 80305 USA.

D. M. M.-P. Schreurs is with the Electronics, Systems, Automation, and Technology–Telecommunications and Microwave Division, Katholieke Universiteit Leuven, B-3001 Leuven, Belgium.

J. Wood is with Agilent Technologies Inc., Santa Rosa, CA 94306 USA.
Digital Object Identifier 10.1109/TMTT.2004.837195

Numerous amplifiers used in wireless communications are operated in a weakly nonlinear regime due to linearity requirements associated with nonconstant-envelope modulation [6]. In this case, the lowest order mixing products will typically dominate. In the fundamental band of frequencies, the lowest order mixing products are the third-order products described above. Thus, in the following, we neglect higher order mixing products, simplifying the treatment considerably.

An amplifier circuit may respond not only to its direct input, but to signals present at frequencies of the mixing products. For example, the amplifier may respond to the sum and difference frequencies of the RF input. The response of the amplifier to the mixing-product signals can induce gain modulation (or memory). This type of distortion is often manifested as a variation in the magnitude and phase of IM3 products with changes in the frequency spacing of the fundamental tones. Examples of mechanisms that induce memory are thermal variations in the device due to time-varying envelope power, and second-order impedances (*RLC* circuits) such as those used in bias circuitry or matching networks [6]–[10], [15]–[18]. As we will show, when coupled with basic knowledge of the physics of a circuit, our mathematical description can readily distinguish IM3 baseband distortion products from those due to gain compression or second harmonic effects due to their different phase symmetries.

III. GAIN MODULATION

A. Theoretical Development

We now develop a simplified description for the IM products at the two IM3 frequencies generated by amplifiers operating in a weakly nonlinear regime. We will focus mainly on interactions at the baseband and second harmonic, and treat the gain compression modeled by the amplifier's third-degree nonlinearity toward the end of the discussion.

We start with the approach of [15] and consider an amplifier driven by two tones of equal amplitude and frequencies ω_1 and ω_2 equally spaced in frequency on either side of a suppressed carrier ω_c . The two signals may have arbitrary phases relative to one another. We express this signal as

$$s(t) = V_0 \cos(\omega_2 t + \phi_2) + V_0 \cos(\omega_1 t + \phi_1). \quad (1)$$

Using the trigonometric identity

$$\cos A + \cos B = 2 \cos\left(\frac{A+B}{2}\right) \cos\left(\frac{A-B}{2}\right) \quad (2)$$

we rewrite (1) as

$$s(t) = 2V_0 \cos\left[\frac{(\omega_2 + \omega_1)t}{2} + \frac{(\phi_2 + \phi_1)}{2}\right] \cdot \cos\left[\frac{(\omega_2 - \omega_1)t}{2} + \frac{(\phi_2 - \phi_1)}{2}\right] \quad (3a)$$

$$= 2V_0 \cos(\omega_m t + \phi_m) \cos(\omega_c t + \phi_c) \quad (3b)$$

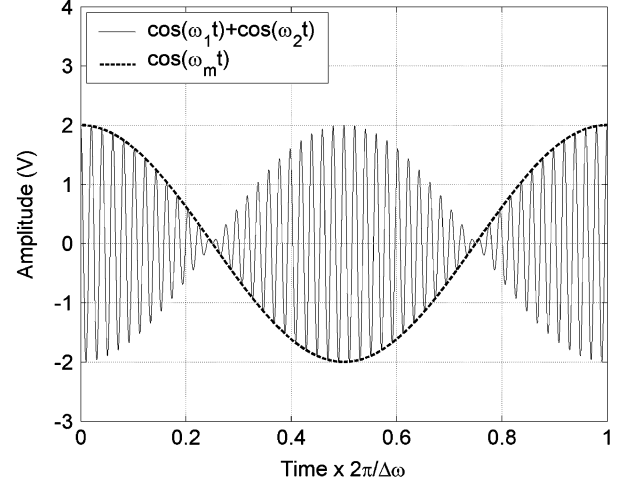


Fig. 1. Sum of two tones at ω_1 and ω_2 (solid line) and their corresponding low-frequency modulating signal ω_m defined in (4b). The time axis is normalized to the envelope period.

where

$$\omega_m = \frac{\omega_2 - \omega_1}{2} \quad (4a)$$

$$\omega_c = \frac{\omega_2 + \omega_1}{2} \quad (4b)$$

$$\phi_m = \frac{\phi_2 - \phi_1}{2} \quad (4c)$$

and

$$\phi_c = \frac{\phi_2 + \phi_1}{2}. \quad (4d)$$

The first cosine term in (3b) modulates the sine-wave carrier at the baseband frequency ω_m , as illustrated in Fig. 1, while the second cosine term corresponds to the suppressed carrier at the frequency between the two sine-wave input signals.

As described in Section II, we assume that the gain of the amplifier is modulated by physical phenomena interacting with the second-order mixing products of the amplifier [4], [5], [8]–[10]. We define this gain modulation function in the time domain as

$$\mathbf{G}(t) = g_0 + g(t) \otimes s^2(t) \quad (5)$$

where g_0 is the linear gain of the amplifier, $g(t)$ is the impulse response of the mechanism that interacts with second-order input signals $s^2(t)$, and \otimes denotes convolution. Circuit elements whose impulse responses have significant energy in the frequency range of the baseband envelope or second harmonic may modulate the gain of the amplifier through (5) even at low input-power levels.

Using (5), we can write the output of the nonlinear circuit as

$$s_{\text{out}}(t) = \mathbf{G}(t)s(t) + g_3 s^3(t) \quad (6)$$

where g_3 is the standard IM3 term due to gain compression. The gain compression term typically comes into play at higher input-signal levels. As we will show, since the IM3 products arising from this term have even symmetry, we often cannot distinguish between IM3 distortion caused by second-harmonic mixing and gain compression without additional knowledge of

the circuit. However, we can almost always distinguish baseband effects from those of second harmonic effects or gain compression due to the difference in phase symmetries. To clearly see these symmetries, we chose a time reference that sets $\phi_1 = \phi_2 = 0^\circ$.

Let us first focus on the source of the baseband and second harmonic effects. Using the trigonometric identities

$$\cos^2 A = \frac{1}{2} (1 + \cos 2A) \quad (7a)$$

and

$$\cos A \cos B = \frac{1}{2} \cos (A + B) + \frac{1}{2} \cos (A - B) \quad (7b)$$

the gain function $G(t)$ in (5) modulates the input signal (3b) as

$$\begin{aligned} s_{\text{out}}(t) &= [g_0 + g(t) \otimes s^2(t)] s(t) \\ &= \left[g_0 + g(t) \otimes V_0^2 \left\{ 1 + \cos [2(\omega_m t + \phi_m)] \right\} \right. \\ &\quad \left. \times \left\{ 1 + \cos [2(\omega_c t + \phi_c)] \right\} \right] s(t) \\ &= \left[g_0 + g(t) \otimes V_0^2 \left\{ \begin{array}{l} 1 + \cos [2(\omega_m t + \phi_m)] \\ + \cos [2(\omega_c t + \phi_c)] \\ + \frac{1}{2} \cos [2(\omega_2 t + \phi_2)] \\ + \frac{1}{2} \cos [2(\omega_1 t + \phi_1)] \end{array} \right\} \right] s(t) \\ &= [g_0 + G(0)V_0^2 + g_{2\omega_m}(t) + g_{2\omega_c}(t) + g_{2\omega_2}(t) \\ &\quad + g_{2\omega_1}(t)] s(t). \end{aligned} \quad (8)$$

We denote

$$G(\omega) = |G(\omega)| \exp [j \angle G(\omega)] \quad (9)$$

as the Fourier transform of $g(t)$. We neglect the linear gain and dc terms and rewrite the last four terms in (8) as four nonlinear complex gain functions

$$\begin{aligned} g_{2\omega_m}(t) &= g(t) \otimes V_0^2 \cos [2(\omega_m t + \phi_m)] \\ &= V_0^2 |G(2\omega_m)| \cos [2(\omega_m t + \phi_m) + \angle G(2\omega_m)] \end{aligned} \quad (10a)$$

$$\begin{aligned} g_{2\omega_c}(t) &= g(t) \otimes V_0^2 \cos [2(\omega_c t + \phi_c)] \\ &= V_0^2 |G(2\omega_c)| \cos [2(\omega_c t + \phi_c) + \angle G(2\omega_c)] \end{aligned} \quad (10b)$$

$$\begin{aligned} g_{2\omega_2}(t) &= g(t) \otimes \frac{V_0^2}{2} \cos [2(\omega_2 t + \phi_2)] \\ &= \frac{V_0^2}{2} |G(2\omega_2)| \cos [2(\omega_2 t + \phi_2) + \angle G(2\omega_2)] \end{aligned} \quad (10c)$$

and

$$\begin{aligned} g_{2\omega_1}(t) &= g(t) \otimes \frac{V_0^2}{2} \cos [2(\omega_1 t + \phi_1)] \\ &= \frac{V_0^2}{2} |G(2\omega_1)| \cos [2(\omega_1 t + \phi_1) + \angle G(2\omega_1)]. \end{aligned} \quad (10d)$$

Each term in (10) acts on different frequency components of $s(t)$, and only three of these four terms will generate IM3 products, as we will see below. Note that the form of these functions

is similar to the Volterra representation in [6], [8]–[10], and [16], but is not device specific. We discuss each in more detail below.

B. Baseband IM Products

We first consider (10a), corresponding to generation of IM3 products due to gain modulation at the baseband envelope frequency $2\omega_m$. As stated previously, the term ω_m in (4c) can be thought of as baseband-frequency modulation of the sine-wave carrier at ω_c . As shown in Fig. 1, the envelope of a two-tone modulated signal will correspond to a frequency of $2\omega_m$, where ω_m is shown by the dashed line in the figure.

Some of the memory-inducing mechanisms mentioned above (bias impedance, thermal changes in the amplifier, electron trapping, etc.) modulate the gain of the amplifier by responding to changes in the average power of the signal at the envelope frequency $2\omega_m$. Intuitively, this makes sense: heating of an amplifier, for example, depends on the average power of the signal it amplifies. Note that the average power in the modulating signal is given by [15]

$$P_{\text{avg}} = V_0^2 \cos^2(\omega_m t + \phi_m) = \frac{V_0^2}{2} \{1 + \cos[2\omega_m t + 2\phi_m]\} \quad (11)$$

which is similar in form to (10a) with the addition of a dc offset $V_0^2/2$.

Using (10a) and (4a)–(4d), we see that IM3 products will be created by gain modulation of the amplifier at baseband frequencies and given by

$$\begin{aligned} s_{2\omega_m}(t) &= V_0^2 |G(2\omega_m)| \cos [2(\omega_m t + \phi_m) + \angle G(2\omega_m)] s(t) \\ &= \frac{V_0^3}{2} |G(2\omega_m)| \left\{ \begin{array}{l} \cos [\omega_2 t + \phi_2 + \angle G(2\omega_m)] \\ + \cos [\omega_1 t + \phi_1 - \angle G(2\omega_m)] \\ + \cos [(2\omega_2 - \omega_1)t + (2\phi_2 - \phi_1) \\ + \angle G(2\omega_m)] \\ + \cos [(2\omega_1 - \omega_2)t + (2\phi_1 - \phi_2) \\ - \angle G(2\omega_m)] \end{array} \right\} \end{aligned} \quad (12)$$

where $G(2\omega_m)$ is the Fourier coefficient of $g_{2\omega_m}(t)$. The last two terms in (12) will contribute to IM3 distortion.

Note that the phase of the baseband gain function $\angle G(2\omega_m)$ is added to the phase of the upper IM3 terms in a positive sense and in a negative sense for the lower IM3 product, as predicted in [7]–[10]. The phases of the upper and lower fundamental tones are also of opposite sign. This phase asymmetry occurs because the gain modulation occurs at the envelope frequency, rather than at the frequency of the excitation tones.

C. Second Harmonic IM Products

We next consider the creation of IM3 products arising from terms at the second harmonic described by (10b)–(10d). Using the same procedure as above, but considering the gain function given in (10b), we write

$$\begin{aligned} s_{2\omega_c}(t) &= V_0^2 |G(2\omega_c)| \cos [2(\omega_c t + \phi_c) + \angle G(2\omega_c)] s(t) \\ &= \frac{V_0^3}{2} |G(2\omega_c)| \end{aligned}$$

$$\times \left\{ \begin{array}{l} \cos [\omega_2 t + \phi_2 + \angle G(2\omega_c)] \\ + \cos [\omega_1 t + \phi_1 + \angle G(2\omega_c)] \\ + \cos [(2\omega_2 + \omega_1)t + (2\phi_2 + \phi_1) \\ + \angle G(2\omega_c)] \\ + \cos [(2\omega_1 + \omega_2)t + (2\phi_1 + \phi_2) \\ + \angle G(2\omega_c)] \end{array} \right\} \quad (13)$$

where $G(2\omega_c)$ is the Fourier coefficient of $g_{2\omega_c}(t)$. We readily note that none of the terms in (13) lie at the IM3 frequencies.

However, the gain functions of (10c) and (10d) will contribute to IM3 distortion. Considering (10c) first,

$$\begin{aligned} s_{2\omega_2}(t) &= \frac{V_0^2}{2} |G(2\omega_2)| \cos [2(\omega_2 t + \phi_2) + \angle G(2\omega_2)] s(t) \\ &= \frac{V_0^3}{4} |G(2\omega_2)| \\ &\times \left\{ \begin{array}{l} \cos [\omega_2 t + \phi_2 + \angle G(2\omega_2)] \\ + \cos [3\omega_2 t + 3\phi_2 + \angle G(2\omega_2)] \\ + \cos [(2\omega_2 + \omega_1)t + (2\phi_2 + \phi_1) \\ + \angle G(2\omega_2)] \\ + \cos [(2\omega_2 - \omega_1)t + (2\phi_2 - \phi_1) \\ + \angle G(2\omega_2)] \end{array} \right\} \quad (14) \end{aligned}$$

where $G(2\omega_2)$ is the Fourier coefficient of $g_{2\omega_2}(t)$. Similarly, (10d) yields

$$\begin{aligned} s_{2\omega_1}(t) &= \frac{V_0^2}{2} |G(2\omega_1)| \cos [2(\omega_1 t + \phi_2) + \angle G(2\omega_1)] s(t) \\ &= \frac{V_0^3}{4} |G(2\omega_1)| \\ &\times \left\{ \begin{array}{l} \cos [\omega_1 t + \phi_1 + \angle G(2\omega_1)] \\ + \cos [3\omega_1 t + 3\phi_1 + \angle G(2\omega_1)] \\ + \cos [(2\omega_1 + \omega_2)t + (2\phi_1 + \phi_2) \\ + \angle G(2\omega_1)] \\ + \cos [(2\omega_1 - \omega_2)t + (2\phi_1 - \phi_2) \\ + \angle G(2\omega_1)] \end{array} \right\} \quad (15) \end{aligned}$$

where $G(2\omega_1)$ is the Fourier coefficient of $g_{2\omega_1}(t)$. The last terms in (14) and (15) contribute to the IM3 distortion. However, here the phase of the upper and lower IM3 products created by (14) and (15) have the same sign. The only IM3 products to have an opposite sign are due to the baseband long-term memory effects.

D. IM Products Due to Gain Compression

The contribution to s_{out} from gain compression can be approximated as

$$\begin{aligned} g_3 s^3(t) &= g_3 V_0^3 [\cos(\omega_2 t + \phi_2) + \cos(\omega_1 t + \phi_1)]^3 \\ &= g_3 V_0^3 \left\{ \begin{array}{l} \frac{9}{4} \cos(\omega_1 t + \phi_1) + \frac{9}{4} \cos(\omega_2 t + \phi_2) \\ + \frac{1}{4} \cos(3\omega_1 t + 3\phi_1) \\ + \frac{1}{4} \cos(3\omega_2 t + 3\phi_2) \\ + \frac{3}{2} \cos [(2\omega_1 - \omega_2)t + (2\phi_1 - \phi_2)] \\ + \frac{3}{2} \cos [(2\omega_2 - \omega_1)t + (2\phi_2 - \phi_1)] \end{array} \right\}. \quad (16) \end{aligned}$$

The last two terms in (16) contribute to IM3 distortion. The magnitudes in (16) will always be equal and the phases will be equal and of the same sign.

Considering (12) and (14)–(16), we clearly see that, as reported in [8]–[10], the IM3 products from baseband mechanisms will have opposite-sign phases through $\angle G(2\omega_m)$. We also see that when $2\omega_1$ and $2\omega_2$ are close in frequency, the IM3 products from second harmonic mechanisms will have same-sign phases since $\angle G(2\omega_2) \approx \angle G(2\omega_1)$. Furthermore, the IM3 products from standard gain compression will also have the same-sign (and always equal) phases. This allows us to easily distinguish baseband mechanisms from mixing at the second harmonic and gain compression.

When baseband effects are present, but do not dominate, both magnitude and phase asymmetry of the IM3 products may occur through the second-harmonic and/or gain compression terms. Such asymmetry can occur, for example, when baseband memory effects such as those arising from a bias network are combined with a reactive second harmonic terminating impedance such as a matching network [8]–[10].

IV. MEASUREMENT RESULTS

A. Fundamental Band of Frequencies

To illustrate the results of Section III, we performed measurements on three different nonlinear circuits, which are: 1) a high-gain 2–6-GHz connectorized microwave power amplifier designed for broad-band telecommunications applications; 2) an on-wafer $0.15 \mu\text{m} \times 100 \mu\text{m}$ GaAs-based metamorphic high electron-mobility transistor (MHEMT) device; and 3) a broad-band (2–22 GHz) GaAs monolithic microwave integrated circuit (MMIC) traveling-wave amplifier (TWA) mounted on a metal shim. The TWA had an external bias circuit and we used needle probes to intentionally introduce long-term memory effects.

We performed two-tone sweeps of the input voltage level and frequency spacing using a vector-signal generator for the excitation and an NVNA for the measurements. The NVNA enables calibrated large-signal measurements of two-port systems, including the magnitude and relative phase of frequency components at the fundamental and harmonic band of frequencies. Unlike a vector network analyzer (VNA), which measures ratios of wave variables, the NVNA measures the forward and reflected wave variables directly. The NVNA simplifies the measurement of both the excitation and IM products of nonlinear amplifiers compared to previously described methods [3], [7]–[9], [13], [14] by providing direct calibrated measurements of the magnitude and phase of the signals.

Fig. 2(a)–(c) shows the amplitude characteristics of the IM3 distortion products at the output port of the three circuits. Note that the two-tone frequency-sweep ranges were chosen to highlight the memory effects of each amplifier circuit.

The lack of variation of the amplitude of the IM3 products with frequency spacing in Fig. 2(a) shows that connectorized amplifier is free of significant memory. We would expect this since its intended use is for broad-band telecommunication signals and was designed to remain distortion free over a broad frequency bandwidth. Conversely, we do see variation in the IM3

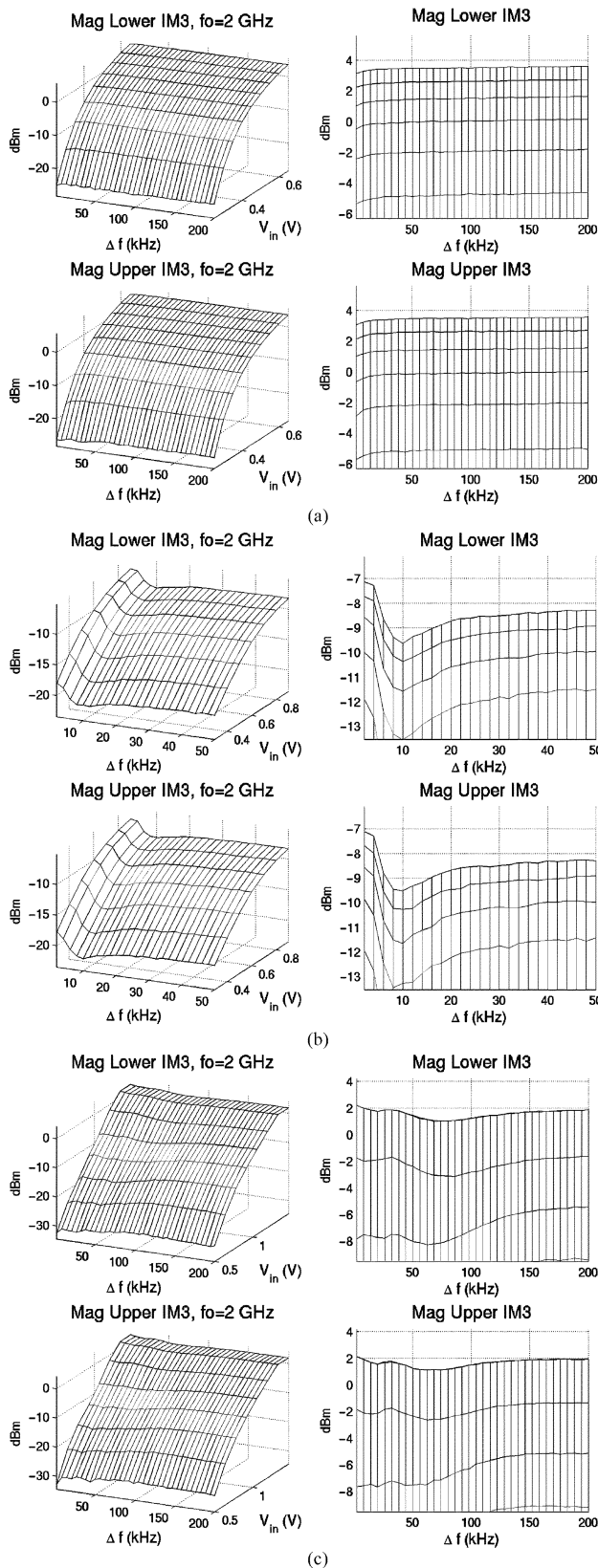


Fig. 2. Magnitude response of the upper and lower IM3 products for three different amplifier types, subjected to two-tone sweeps of input voltage level V_{in} and tone spacing Δf . (a) Connectorized high-gain 2-6-GHz amplifier. (b) GaAs-based on-wafer MHEMT structure. (c) Broad-band TWA with external bias circuit.

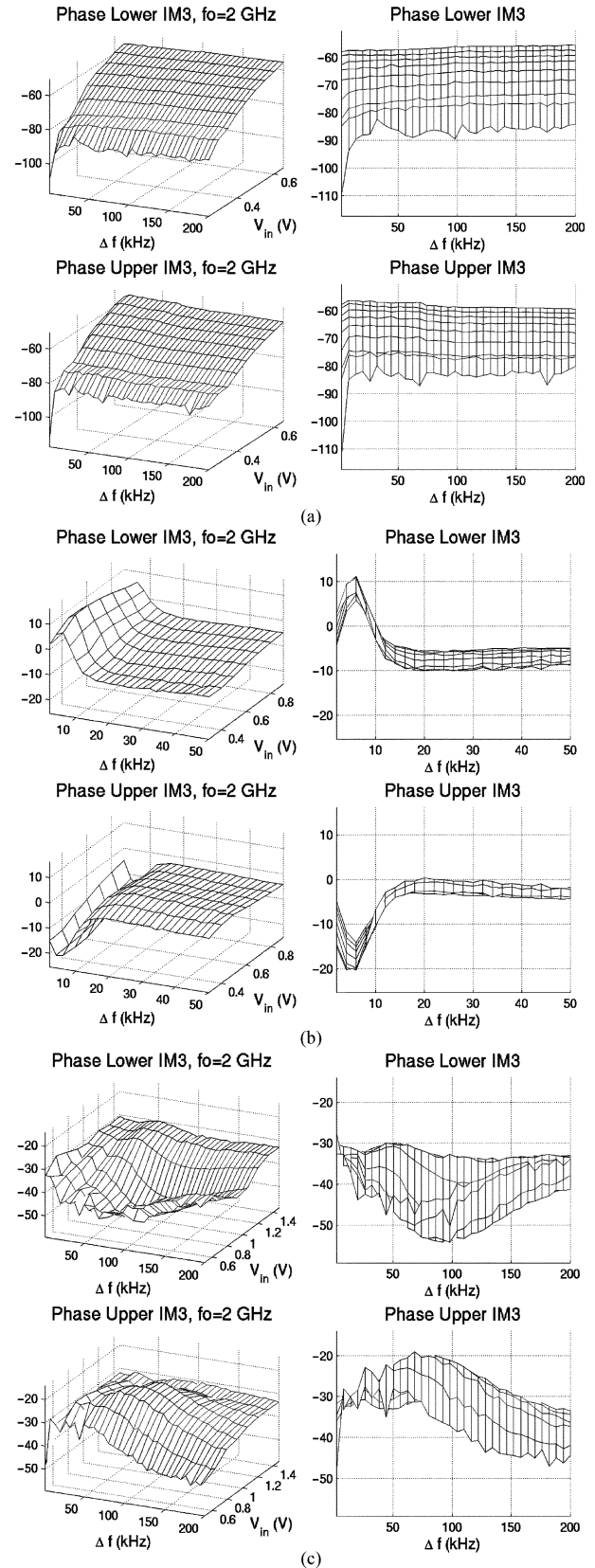


Fig. 3. Phase response (in degrees) of the upper and lower IM3 products for three different amplifier types, subjected to two-tone sweeps of input voltage level V_{in} and tone spacing Δf . (a) Connectorized high-gain 2-6-GHz amplifier. (b) GaAs-based on-wafer MHEMT structure. (c) Broad-band TWA with external bias circuit.

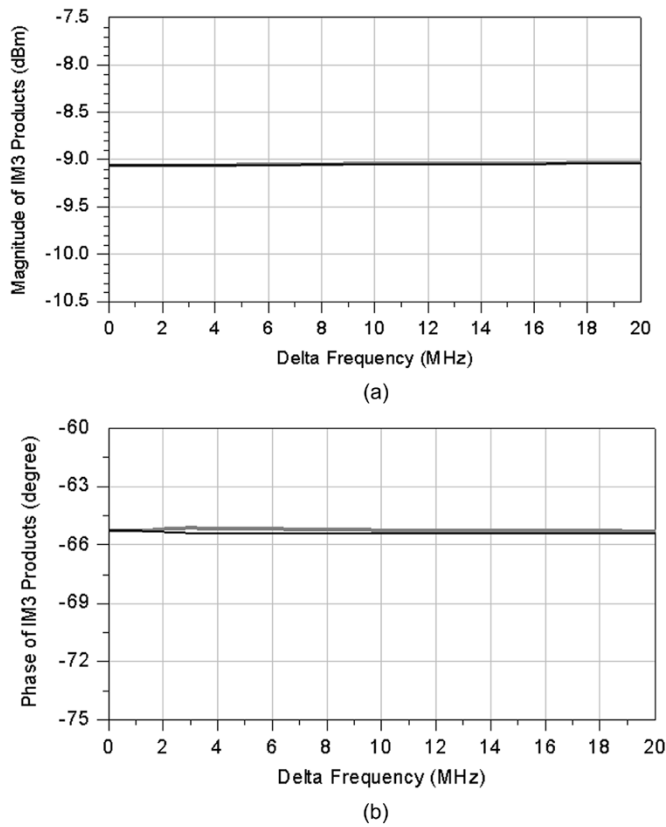


Fig. 4. Simulation of an FET circuit showing: (a) magnitude and (b) phase values of the IM3 products as a function of frequency with an ideal dc block used as a bias network. The lower IM3 product is black. The upper IM3 product is gray.

product amplitude in Fig. 2(b) and (c), indicating the presence of memory in the MHEMT and TWA circuits.

Fig. 3(a)–(c) shows the phase of the IM3 products at the output port of the three circuits. We chose a reference time that sets $\phi_1 = \phi_2 = 0^\circ$. We detrended the relative phases to retain the time delay and linear distortion through the device using the procedure of [12]. We first found the time interval that best aligned the measured input phases to their specified values of 0° . We then used the same time interval to time align the output voltage phases.

The connectorized amplifier [see Fig. 3(a)], whose IM3 products had a flat amplitude with frequency spacing, also shows little variation in phase, as predicted by (10a)–(10d). The MHEMT and TWA clearly show the phase sign reversal predicted in (12) and [7]–[10], indicating prominent baseband memory effects.

We can use our knowledge of the physical attributes of the circuits and simulations to understand the source of these memory effects. Since the HEMT device is of small size, we do not expect significant heating or power dissipation and, thus, we do not expect that the memory arises from thermal heating.

In fact, Figs. 4 and 5 show that the bias networks we used in the measurements of Figs. 2(b) and 3(b) may well be the dominant memory-inducing mechanism. Here, we see the simulated IM3 magnitude and phase of a transistor-level model of a field-effect transistor (FET) amplifier circuit embedded between two bias networks. We modeled the amplifier circuit using the

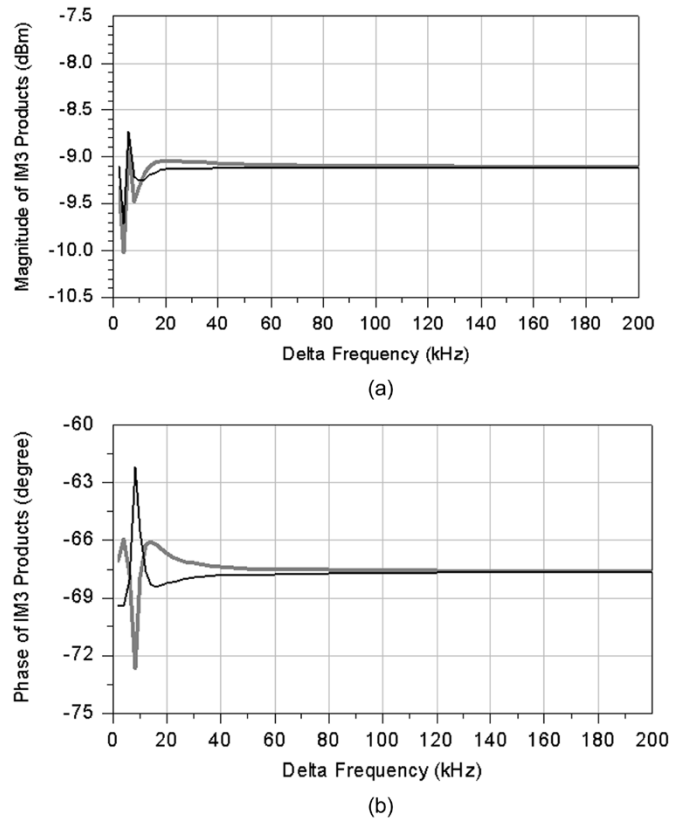


Fig. 5. Simulation an FET circuit showing: (a) magnitude and (b) phase values of the IM3 products as a function of frequency with a bias tee that induces long-term memory over a narrow frequency range. The lower IM3 product is black. The upper IM3 product is gray. Bias circuit values were taken from a manufacturer's specifications.

“Root” model [19] for an FET with customized parasitic networks [20]. The Root model uses a first-order function to interpolate between dc and RF drain current models. In Fig. 4, we represent the bias networks by ideal, but nonphysical, dc blocks and feed components. In this case, the bias networks do not present a frequency-dependent impedance and, thus, will not introduce any baseband memory effects; dispersion in the FET model is not observed as the presented impedances do not change with frequency.

In Fig. 5, the bias networks are represented by a complex equivalent circuit provided by the manufacturer of the bias tee that we used in the MHEMT measurements. Note a spike in the IM3 products at a frequency spacing of approximately 10 kHz, near the frequency spacing of a spike in the amplitude and phase of the IM3 products for the MHEMT in Figs. 2(b) and 3(b) (recall that the TWA measurements used a needle-probe bias network and, thus, do not show the spike at this frequency).

B. Second Harmonic Measurements

NVNAs typically do not measure signals at baseband frequencies without the use of additional external instrumentation [21]. This restriction is imposed by both the directional couplers and calibrations of the instrument. However, NVNA measurements at the second harmonic ($2\omega_1$ and $2\omega_2$) can provide useful information on the nonlinear system under test and demonstrate some of the IM phenomena discussed in previous sections.

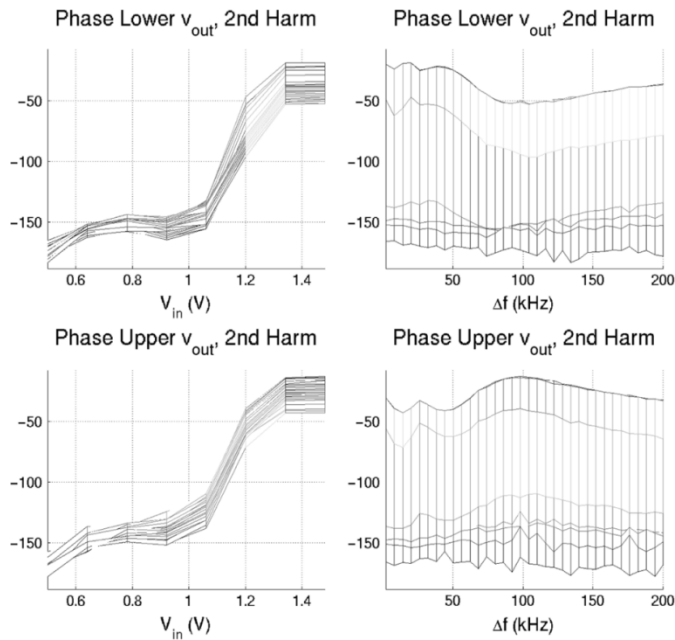


Fig. 6. Phase response (in degrees) of the lower and upper output voltage at the second harmonic for the broad-band TWA.

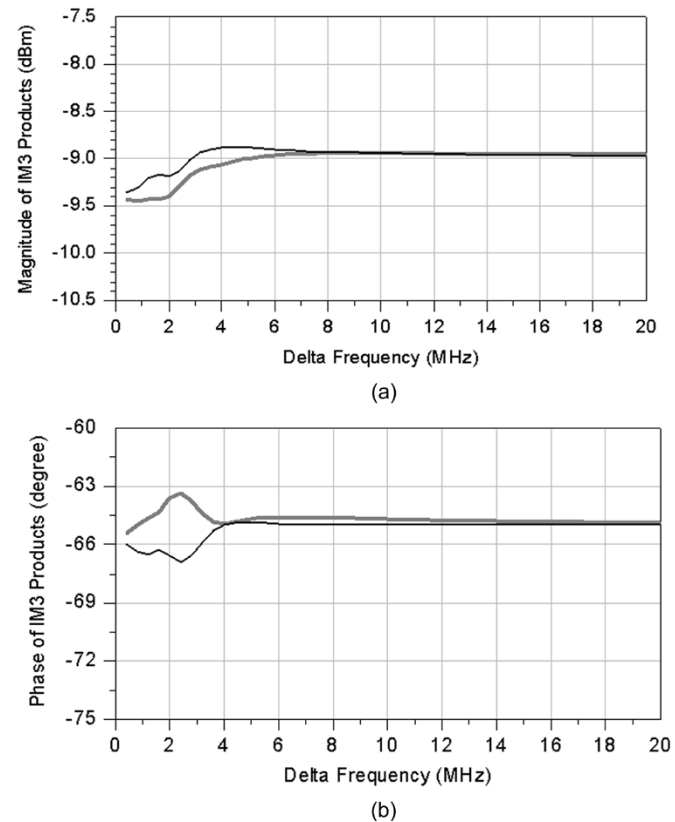


Fig. 7. Simulation of the TWA circuit showing: (a) magnitude and (b) phase values of the IM3 products as a function of frequency with a bias tee that induces long-term memory over a broad frequency range. Lower IM3 product is black, upper IM3 product is gray. Bias-circuit values were taken from manufacturer's specifications.

As an example, the phase of the output voltage at $2\omega_1$ and $2\omega_2$ for the TWA is shown in Fig. 6. We see that, while the phases are of the same sign as predicted by (14) and (15), they

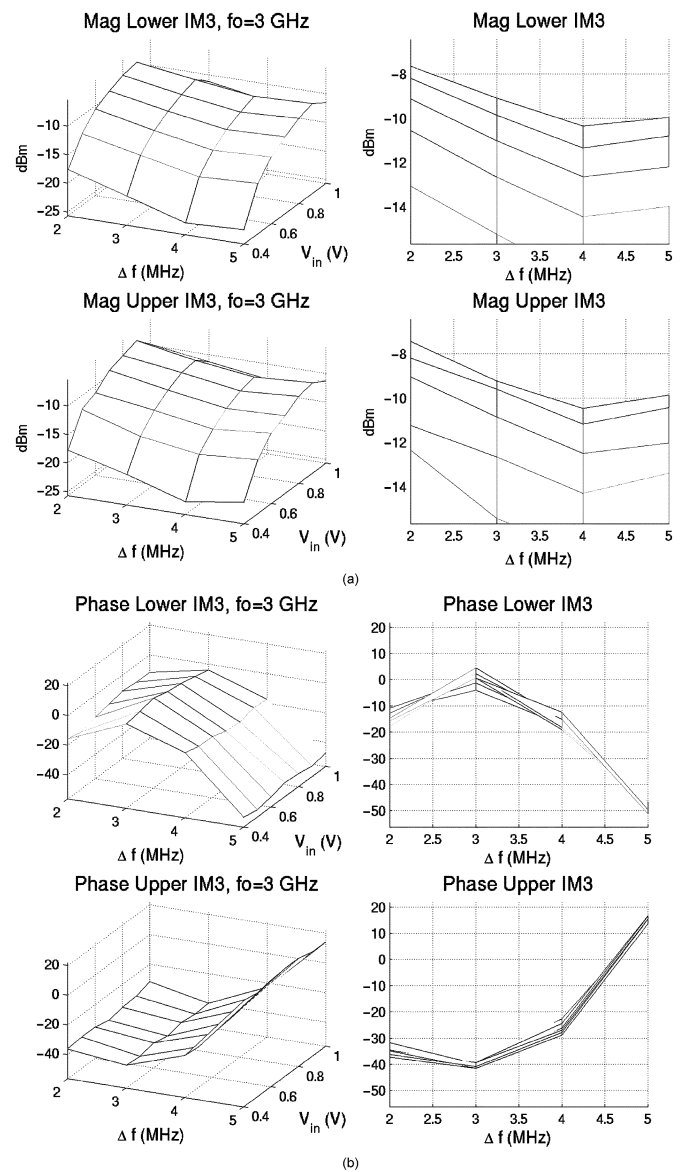


Fig. 8. NVNA measurements made using the extended bandwidth technique. (a) Magnitude and (b) phase (degrees) of the IM3 products for the MHEMT using the bias tee whose response is given in Fig. 7 (from [24]).

are also somewhat different in absolute value, enabled by the independence of the quantities in (14) and (15).

C. Long-Term Memory Effects With Broad Frequency Response

Fig. 7 shows the simulated IM3 response of the amplifier circuit model used in Figs. 4 and 5, but here we use the manufacturer's values for a bias tee whose components induce memory over a much broader frequency range. To completely characterize the IM distortion due to this bias circuit, we would need to use two-tone frequency spacings wider than normally possible with our NVNA because of the 8-MHz IF bandwidth of our instrument. (Note that not all NVNAs suffer from this bandwidth limitation, the cause of which is described in [22]. However, at present, calibration of instruments with wider IF bandwidths requires that one channel of the sampling frequency converter be assumed to be ideal [23].)

In [24], we developed a new measurement method to extend the measurement range of our instrument. Our method [24] is based on a series of calibrated single-frequency NVNA measurements at the frequency of each excitation tone and IM product of interest. Phase alignment is provided by a calibration signal that consists of a set of small “tickler” tones generated at the input of the circuit. Ticklers are generated at the IM frequencies along with the large-signal two-tone excitation. We determine the phases of the IM products from the relative input-to-output phase measured by the NVNA and the known phases of the input signal.

We applied our NVNA bandwidth-extension procedure to the MHEMT device with the bias tee modeled in the simulations in Fig. 7. We swept the input voltage from 0.4 to 1.0 V and the two-tone frequency spacing from 2 to 5 MHz, producing IM3 products spaced from 6 to 15 MHz. We show the magnitude and phase of the measured IM3 products in Fig. 8(a) and (b), respectively. Due to the bias tee’s broad frequency response, we expect to see variation in magnitude and phase of the IM products at wider frequency spacings. These effects are readily apparent in our measurements as the two-tone frequency spacing is increased. Note also that the phases are of opposite sign again, confirming that we are indeed seeing a baseband memory effect.

V. CONCLUSION

We have presented an intuitive unified description to aid in understanding IM3 distortion arising from both baseband and second harmonic memory. Our description is based on the product of a second-order gain modulation function with a two-tone excitation signal. This description reverts to the memoryless case when no long-term mechanisms are present. We verified our description through illustrative large-signal NVNA measurements of nonlinear amplifier and transistor circuits.

We also utilized a technique for increasing the measurement bandwidth of our NVNA for two-tone IM measurements. We demonstrated that the contributions to long-term memory that have a frequency response greater than the IF bandwidth of our NVNA may be identified using the additional measurement bandwidth.

REFERENCES

- [1] C. P. Silva, A. A. Moulthrop, and M. S. Muha, “Introduction to polyspectral modeling and compensation techniques for wideband communication systems,” in *58th Automatic RF Techniques Group Conf. Dig.*, San Diego, CA, 2001, pp. 1–15.
- [2] C. J. Clark, G. Chriskos, M. S. Muha, A. A. Moulthrop, and C. P. Silva, “Time-domain envelope measurement technique with application to wideband power amplifier modeling,” *IEEE Trans. Microwave Theory Tech.*, vol. 46, pp. 2531–2540, Dec. 1998.
- [3] H. Ku, M. D. McKinley, and J. S. Kenney, “Quantifying memory effects in RF power amplifiers,” *IEEE Trans. Microwave Theory Tech.*, vol. 50, pp. 2843–2849, Dec. 2002.
- [4] P. M. Asbeck, H. Kobayashi, M. Iwamoto, G. Hanington, S. Nam, and L. E. Larson, “Augmented behavioral characterization for modeling the nonlinear response of power amplifiers,” in *IEEE MTT-S Int. Microwave Symp. Dig.*, June 2002, pp. 135–138.
- [5] P. Draxler, I. Langmore, T. P. Hung, and P. M. Asbeck, “Time domain characterization of power amplifiers with memory effects,” in *IEEE MTT-S Int. Microwave Symp. Dig.*, June 2003, pp. 803–806.

- [6] J. F. Sevic, K. L. Burger, and M. B. Steer, “A novel envelope-termination load-pull method for ACPR optimization of RF/microwave power amplifiers,” in *IEEE MTT-S Int. Microwave Symp. Dig.*, June 1998, pp. 723–726.
- [7] J. H. K. Vuolevi, T. Rahkonen, and J. P. A. Manninen, “Measurement technique for characterizing memory effects in RF power amplifiers,” *IEEE Trans. Microwave Theory Tech.*, vol. 49, pp. 1383–1389, Aug. 2001.
- [8] N. Borges de Carvalho and J. C. Pedro, “A comprehensive explanation of distortion sideband asymmetries,” *IEEE Trans. Microwave Theory Tech.*, vol. 50, pp. 2090–2101, Sept. 2002.
- [9] J. Brinkhoff and A. E. Parker, “Effect of baseband impedance on FET intermodulation,” *IEEE Trans. Microwave Theory Tech.*, vol. 51, pp. 1045–1051, Mar. 2003.
- [10] V. Aparin and C. Persico, “Effect of out-of-band terminations on intermodulation distortion in common-emitter circuits,” in *IEEE MTT-S Int. Microwave Symp. Dig.*, June 1999, pp. 977–980.
- [11] T. Van den Broeck and J. Verspecht, “Calibrated vectorial nonlinear-network analyzers,” in *IEEE MTT-S Int. Microwave Symp. Dig.*, June 1994, pp. 1069–1072.
- [12] K. A. Remley, D. F. Williams, D. Schreurs, G. Loglio, and A. Cidronali, “Phase detrending for measured multisine signals,” in *61st Automatic RF Techniques Group Conf. Dig.*, Philadelphia, PA, 2003, pp. 73–83.
- [13] B. Kim, Y. Yang, J. Cha, Y. Y. Woo, and J. Yi, “Measurement of memory effect of high-power Si LDMOSFET amplifier using two-tone phase evaluation,” in *58th Automatic RF Techniques Group Conf. Dig.*, San Diego, CA, 2001, pp. 159–167.
- [14] J. Dunsmore and D. Goldberg, “Novel two-tone intermodulation phase measurement for evaluating amplifier memory effects,” in *33rd Eur. Microwave Conf. Dig.*, Oct. 2003, pp. 235–238.
- [15] S. C. Cripps, *RF Power Amplifiers for Wireless Communications*. Norwood, MA: Artech House, 1999.
- [16] S. Maas, *Nonlinear Microwave Circuits*. Norwood, MA: Artech House, 1988.
- [17] A. E. Parker and J. G. Rathmell, “Measurement and characterization of HEMT dynamics,” *IEEE Trans. Microwave Theory Tech.*, vol. 49, pp. 2105–2111, Nov. 2001.
- [18] —, “Bias and frequency dependence of FET characteristics,” *IEEE Trans. Microwave Theory Tech.*, vol. 51, pp. 588–592, Feb. 2003.
- [19] D. E. Root, “A measurement-based FET model improves CAE efficiency,” *Microwave J.*, pp. 126–139, Sept. 1991.
- [20] J. Wood and D. E. Root, “Bias-dependent linear scalable millimeter-wave FET model,” *IEEE Trans. Microwave Theory Tech.*, vol. 48, pp. 2352–2360, Dec. 2000.
- [21] D. J. Williams, J. Leckey, and P. J. Tasker, “A study of the effect of envelope impedance on intermodulation asymmetry using a two-tone time domain measurement system,” in *IEEE MTT-S Int. Microwave Symp. Dig.*, June 2002, pp. 1841–1844.
- [22] P. Crama and Y. Rolain, “Broad-band measurement and identification of a Wiener–Hammerstein model for an RF amplifier,” in *60th Automatic RF Techniques Group Conf. Dig.*, Washington, DC, 2003, pp. 49–57.
- [23] J. Verspecht, “The return of the sampling frequency convertor,” in *62nd Automatic RF Techniques Group Conf. Dig.*, Boulder, CO, 2004, pp. 155–161.
- [24] K. A. Remley, D. Schreurs, D. F. Williams, and J. Wood, “Extended NVNA bandwidth for long-term memory measurements,” in *IEEE MTT-S Int. Microwave Symp. Dig.*, June 2004, pp. 1739–1742.



Kate A. Remley (S’92–M’99) was born in Ann Arbor, MI, in 1959. She received the Ph.D. degree in electrical and computer engineering from Oregon State University, Corvallis, in 1999.

From 1983 to 1992, she was a Broadcast Engineer in Eugene, OR. From 1989 to 1991, she was Chief Engineer of an AM/FM broadcast station. In 1999, she joined the Radio-Frequency Technology Division, National Institute of Standards and Technology (NIST), Boulder, CO, as an Electronics Engineer. Her research activities focus on development of

metrology for wireless systems, and characterizing the link between nonlinear circuits and system performance.

Dr. Remley was the recipient of the Department of Commerce Silver Medal and the Automatic RF Techniques Group (ARFTG) Best Paper Award.



Dylan F. Williams (M'80–SM'90–F'02) received the Ph.D. degree in electrical engineering from the University of California at Berkeley, in 1986.

In 1989, he joined the Electromagnetic Fields Division, National Institute of Standards and Technology (NIST), Boulder, CO, where he develops metrology for the characterization of MMICs and electronic interconnects. He has authored or coauthored over 80 technical papers.

Dr. Williams is an associate editor for the IEEE TRANSACTIONS ON MICROWAVE THEORY AND TECHNIQUES. He was the recipient of the Department of Commerce Bronze and Silver Medals, the Electrical Engineering Laboratory's Outstanding Paper Award, two ARFTG Best Paper Awards, the ARFTG Automated Measurements Technology Award, and the IEEE Morris E. Leeds Award.



Dominique M. M.-P. Schreurs (S'90–M'97–SM'02) received the M.Sc. degree in electronic engineering and Ph.D. degree from the Katholieke Universiteit (K.U.) Leuven, Leuven, Belgium, in 1992 and 1997, respectively.

She is currently a Post-Doctoral Fellow of the Fund for Scientific Research–Flanders and a Visiting Assistant Professor at K.U. Leuven. She has been a Visiting Scientist with Agilent Technologies Inc., Eidgenössische Technische Hochschule (ETH) Zurich, and the National Institute of Standards and

Technology (NIST). Her main research interest is the use of large-signal vector measurements for the characterization and modeling of nonlinear microwave devices.

Dr. Schreurs is vice-chair of the IEEE MTT-11 Committee on Microwave Measurements. She serves as workshop chair on the Executive Committee of the ARFTG.



John Wood (M'87–SM'03) received the B.Sc. and Ph.D. degrees in electrical and electronic engineering from The University of Leeds, Leeds, U.K., in 1976 and 1980, respectively.

From 1983 to 1997, he was a member of the academic staff with the University of York, York, U.K., where he was responsible for teaching and research in solid-state electronics and microwave device and circuit technology. In 1997, he joined the Microwave Technology Center, Agilent Technologies Inc. (formerly the Hewlett-Packard Company),

Santa Rosa, CA. He is currently with the Computer-Aided Engineering, Modeling, and Advanced Characterization Group. He has authored or coauthored approximately 70 papers. His recent research has included the investigation and development of analytic large-signal FET models, and bias-dependent linear FET models for millimeter-wave applications, HBT modeling, and nonlinear behavioral modeling using NVNA measurements, and nonlinear system identification techniques.